ISSN 0915-633

NATIONAL INSTITUTE FOR FUSION SCIENCE

High-Energy Acceleration of an Intense Negative Ion Beam

Y. Takeiri, A. Ando, O. Kaneko, Y. Oka, K. Tsumori, R. Akiyama, E. Asano, T. Kawamoto, M. Tanaka and T. Kuroda

(Received - Jan. 31, 1995)

NIFS-338 Feb. 1995

RESEARCH REPORT
NIFS Series

NAGOYA, JAPAN

High-Energy Acceleration of an Intense Negative Ion Beam

Y. Takeiri, A. Ando, O. Kaneko, Y. Oka, K. Tsumori, R. Akiyama,
E. Asano, T. Kawamoto, M. Tanaka*, and T. Kuroda

National Institute for Fusion Science, Nagoya 464-01, Japan

* *Hitachi Research Laboratory, Hitachi Ltd., Hitachi 316, Japan*

Abstract

A high-current H^- ion beam has been accelerated with the two-stage acceleration. A large negative hydrogen ion source with an external magnetic filter produces more than 10 A of the H^- ions from the grid area of 25 cm x 50 cm with the arc efficiency of 0.1 A/kW by seeding a small amount of cesium. The H^- ion current increases according to the 3/2-power of the total beam energy. A 13.6 A of H^- ion beam has been accelerated to 125 keV at the operational gas pressure of 3.4 mTorr. The optimum beam acceleration is achieved with nearly the same electric fields in the first and the second acceleration gaps on condition that the ratio of the first acceleration to the extraction electric fields is adjusted for an aspect ratio of the extraction gap. The ratio of the acceleration drain current to the H^- ion current is more than 1.7. That is mainly due to the secondary electron generated by the incident H^- ions on the extraction grid and the electron suppression grid. The neutralization efficiency was measured and agrees with the theoretical calculation result.

Keywords :

negative ion source, high-energy acceleration, negative-ion-based NBI external magnetic filter, cesium seeding, neutralization efficiency

1. Introduction

In the next step fusion experimental devices, a high-energy, more than several hundreds keV, neutral beam injection (NBI) system is required, where the negative ion beam is used for its high neutralization efficiency at the high beam energies. The ITER (International Thermonuclear Experimental Reactor) - NBI system is engineeringly designed with the injection energy of 1.0 MeV using the multi-stage electrostatic acceleration [1]. For recent several years, high-current negative ion sources which enable a real injector design have been developed in the cesium-seeded operation [2-7]. On the other hand, the high-energy acceleration up to 400 keV of the H^- ions has been demonstrated with the two-stage acceleration of a small current of 0.18 A [8], and a 2 A of D^- ion beam has been accelerated to 105 keV with the single-stage acceleration [9].

A negative-ion based NBI system is planned in the Large Helical Device (LHD) project [10], which injects 20 MW of hydrogen/deuterium beams with the energy of 125(H)/250(D) keV [11]. For this system, a 125 keV-45 A hydrogen negative ion source should be developed. Recently, we have developed a high-current negative ion source which produced a 47 keV-16.2 A of H^- ion beam with a single-stage acceleration [6,7]. This ion source has 1/3 of grid area of the ion source required for the LHD-NBI system, and is operated at the high arc efficiency of 0.1 A/kW at the low gas pressure of 3.5 mTorr. In order to demonstrate and to investigate the high-energy acceleration of an intense negative ion beam, we have added a grid to this ion source accelerator for the two-stage acceleration of more than 10 A of negative ion beams. In this paper, the experimental results of the high-energy negative-ion

acceleration are presented in detail.

2. Experimental Set-Up

Figure 1 (a) shows an external-filter type 1/3-scaled negative ion source used for the acceleration experiments. The detailed structure is described in ref. 6. The arc chamber has the dimensions of 35 cm x 62 cm in cross section and 21 cm in depth and the beam extraction area is 25 cm x 50 cm, which corresponds to a 1/3 scale-model of the ion source in the LHD-NBI system. A strong external magnetic filter field in the X-direction in Fig. 1 (a) is generated in wide area in front of the plasma grid by a pair of permanent magnet rows facing each other with the distance of 35 cm.

The grid arrangement along the beam axis is shown in Fig. 1 (b). The plasma grid (PG) is made of molybdenum and thermally insulated for the cesium-mode operation. The aperture diameter of the plasma grid is 11.3 mm and the number of the aperture is 522 (18 x 29). The extraction grid (EG) is thick, 11 mm, because of the embedded large permanent magnets which generate the strong magnetic field in the Y-direction for the electron suppression. The gap length between the PG and the EG is 3 or 5 mm in the experiments. The electron suppression grid (SG) has the same potential as the EG. The first acceleration gap length between the SG and the acceleration grid (AG) is 16 mm and the second acceleration gap length between the AG and the grounded grid (GG) is 32 mm. The beamlets are not focused, that is, parallel beams. The grids are edge-cooled except for the EG which is water-cooled in the vicinity of the apertures. Thus, the pulse length is short, less than 300 ms. The electrical connections of the power supplies are also indicated

in Fig. 1 (b).

The ion source is attached to the negative-ion-beam teststand [12-14] via a gate-valve of 800 mm in diameter. A horizontal beam limiter (in the X-direction) of 310 mm in width is placed at the distance of 4 m from the ion source. The negative ion current is thermally measured by a movable multi-channel calorimeter array placed 5 m downstream of the ion source. There are 15 channels in the horizontal (X) direction and 25 channels in the vertical (Y) direction. The teststand chamber is evacuated by a cryopump with the pumping speed of 450 m^3/s.

3. Experimental Results

3.1. High-current negative-ion beam acceleration

The extraction, the first acceleration and the second acceleration voltages, V_{ext}, V_{acc1} and V_{acc2}, respectively, were varied as the measured negative ion currents would show the maximum. Figure 2 (a) shows the H^- ion current, I_{H^-}, and the second acceleration drain current, I_{acc2}, as a function of the arc power at the gas pressure of 3.4 mTorr. The H^- ion beam energy is 110 to 125 keV and the extraction gap length is 3 mm. The H^- ion current accelerated with the two stages increases with an increase in the arc power at the arc efficiency (the ratio of the H^- ion current to the arc power) of around 0.1 A/kW. The I_{acc2} also increases proportionally to the arc power and the ratio of the second acceleration current to the H^- ion current, I_{acc2}/I_{H^-}, is 1.7 to 2.4. The ratio of the extraction current to the H^- ion current, I_{ext}/I_{H^-}, is relatively small and 2.2 to 3.2. The first acceleration current, I_{acc1}, is a little larger than the I_{acc2} by about 5 % or less. In the case of the single-stage acceleration, the arc efficiency was also around 0.1 A/kW [6]. Thus, it is thought that there

is almost no loss of the H^- ions during the second acceleration. As shown in Fig. 2 (a), however, the arc efficiency is degraded at the arc power of higher than 120 kW. This is caused by the shortage of the acceleration voltage against the higher H^- ion currents at the higher arc powers. Figure 2 (b) shows the H^- ion current as a function of the total beam energy for the same conditions in Fig. 2 (a). A dashed line indicates the 3/2-power dependency on the beam energy. It is found that the accelerated H^- ion current is closely related with the total beam energy. The maximum H^- ion current at each beam energy increases according to the 3/2-power of the beam energy. The H^- ion currents are extracted also according to the Child-Langmuir 3/2-power law of the extraction voltage [6]. In the experiments, the maximum applied voltage to the ion source was limited to 125 kV, and a 13.6 A of H^- ion current was accelerated to 125 keV.

3.2. Gas pressure dependence

The low gas pressure operation is essential for the high-energy negative ion beam acceleration, because the stripping loss of the negative ions results in the lower acceleration efficiency and the high thermal load of the grids by the dissociated electrons. Figure 3 (a) shows the arc efficiency of the H^- ions as a function of the gas pressure. The arc power is 90 to 100 kW and the beam energy is 113 keV. The extraction gap length is 3 mm. At the gas pressure of 2.5 mTorr the arc efficiency is still 0.1 A/kW. The I_{ext}/I_{H^-} and the I_{acc2}/I_{H^-} as a function of the gas pressure are shown in Fig. 3 (b). The electrons extracted together with the H^- ions are much suppressed even at this low gas pressure. The I_{acc2} is almost the same as or several % lower than the I_{acc1}.

Figure 4 shows the simulation results of the gas pressure distribution and the survival H^- ion ratio without the stripping loss in the accelerator using the Monte-Carlo gas flow calculation code [15]. The gas temperature is assumed to be constant, 300 K. The gas flow rate is 19 Torr l/s and the calculated gas pressure in the arc chamber is 3.3 mTorr. The total stripping loss of the H^- ion beam is calculated at 20 %. The stripping losses during the first and the second accelerations of the H^- ions are not so large, about 5 % and 3 %, respectively, of the H^- ion current at the plasma grid aperture. The H^- ion current accelerated to the full-energy without the stripping loss is calculated at about 95 % of the calorimetrically estimated H^- ion current. Therefore, the operational gas pressure of 3.3 mTorr is low enough for the neutral beam application of this H^- ion source.

3.3. Beam profile

The two-dimensional beam profile can be obtained by moving the calorimeter array vertically (in the Y-direction in Fig. 1 (a)). Figure 5 shows the contours of the H^- ion beam current density measured by the movable calorimeter array. The arc power is 90 kW. The beam energy is 109 keV and the total H^- ion current is 9.6 A. The extraction gap length is 5 mm. The beam is shifted downward by about 4 cm. Since the external magnetic filter field is applied horizontally (in the X-direction) over the beam acceleration region and the beam drift region, the H^- ions are deflected vertically by this magnetic field. In general, the deflection angle is proportional to the line-integrated transverse magnetic field. In this source, the line-integrated field strength in the beam acceleration and drift regions is about 540 G cm. Thus, the beam deflection angle is

estimated at 11.3 mrad and the beam would shift by 5.7 cm at the position of the calorimeter array. The actual beam shift is less than the estimated one. The geometrical accuracy in installing the ion source may influence the beam shift. As shown in Fig. 5, the beam uniformity is not so good in the vertical direction. In the cesium mode operation, the H^- ion production is influenced by the PG temperature and the cesium coverage on the PG. These may cause the beam ununiformity. The optimization of the cesium mode operation is required.

The horizontal (X) profile of the H^- ion beam is shown in Fig. 6. The arc power is 88 kW, the total H^- ion current is 8.5 A, and the beam energy is 110 keV. The extraction gap length is 5 mm. The horizontal positions of 17.5 cm and -17.5 cm are located outer than those of the horizontal beam limiter of 31 cm in width. The calculated beam profile using the multi-gaussian beamlets (18 x 29) with the divergent angle of 16 mrad is also shown by a dotted line in the figure. The measured beam profile is in relatively good agreement with the calculated one. The beam divergent angle is large compared with that of the reported single beamlet [8,16]. The direction of the magnetic field produced by the permanent magnets embedded in the extraction grid is in the opposite direction line by line along the vertical direction. As a result, the horizontal deflection of the beamlets is occurred in the opposite direction line by line along the vertical direction. The horizontal deflection of a line of beamlets is calculated at 5-7 mrad in this case, and the beam divergent angle is estimated at 14 mrad or less when the alternate horizontal deflection is took into account. The beam ununiformity also could have an influence on the estimation of divergent angle.

3.4. Dependence on electric field ratio

The accelerated H^- ion beam property is influenced by the ratio of the second to the first acceleration electric fields, E_{acc2}/E_{acc1}. Figure 7 (a) shows the FWHM of the horizontal profile, H_{FWHM}, as a function of the E_{acc2}/E_{acc1}. The extraction gap length is 3 mm. The V_{ext} and the V_{acc1} are constant, 6.7 and 35 kV, respectively, that corresponds to the ratio of the first acceleration to the extraction electric fields, E_{acc1}/E_{ext}, of 0.98. The E_{acc2}/E_{acc1} was changed by only the V_{acc2}. The arc power is 90 kW and the operational gas pressure is 3.4 mTorr. The H_{FWHM} shows the minimum at around 1.0 of the E_{acc2}/E_{acc1}, although the dependency of the H_{FWHM} on the E_{acc2}/E_{acc1} is week. The H^- ion current measured by the calorimeter array, I_{H^-}, and the I_{acc2}/I_{H^-} as a function of the E_{acc2}/E_{acc1} is shown in Fig. 7 (b). The I_{acc2}/I_{H^-} has a nearly the same dependency as that of the H_{FWHM} on the E_{acc2}/E_{acc1}. The dependency of the I_{H^-} on the E_{acc2}/E_{acc1} is also week and the I_{H^-} shows the maximum around 1.0 of the E_{acc2}/E_{acc1}.

The H_{FWHM} as a function of the ratio of the E_{acc1}/E_{ext} is shown in Fig. 8 (a), for the E_{acc2}/E_{acc1} of 0.9, 1.05 and 1.15. The V_{ext} is constant, 6.7 kV. The other conditions are the same as those in Fig. 7. Figures 8 (b) and (c) show the I_{H^-} and the I_{acc2}/I_{H^-} as a function of the E_{acc1}/E_{ext}, respectively, for the same E_{acc2}/E_{acc1} as those in Fig. 8 (a). The H_{FWHM} and the I_{acc2}/I_{H^-} show the broad minimums at 0.9-1.1 of the E_{acc1}/E_{ext}, where the I_{H^-} shows the broad maximum. It is observed that the E_{acc2}/E_{acc1} should be increased for a good beam optics when the E_{acc1} is weak compared with the E_{ext}.

Figure 9 (a) shows the H_{FWHM} as a function of E_{acc2}/E_{acc1} in the

case of the extraction gap length of 5 mm. The V_{ext} and the V_{acc1} are 8.2 kV and 31 kV, respectively, that corresponds to the E_{acc1}/E_{ext} of 1.18. The arc power is 90 kW. The arc efficiency and the I_{acc2}/I_{H^-} as a function of the E_{acc2}/E_{acc1} are shown in Fig. 9 (b) for the same conditions as those in Fig. 9 (a). The H_{FWHM} shows the minimum at the E_{acc2}/E_{acc1} of around 1.15, where the arc efficiency and the I_{acc2}/I_{H^-} shows the maximum and the minimum, respectively. In the case of the extraction gap length of 5 mm, the optimum E_{acc1}/E_{ext} is higher than that in the case of 3 mm. However, the optimum E_{acc2}/E_{acc1} is still 1.0-1.1 at the E_{acc1}/E_{ext} of about 1.4 or more.

3.5. Neutralization efficiency

The high-energy H^- ion beam was transported to a neutral beam dump located 13.6 m downstream from the ion source via a neutralizer. In order to measure the neutralization efficiency, hydrogen gas was fed into the neutralizer and the residual ion bending magnet was operated. There are many thermocouples on the neutral beam dump. The ratio of the temperature rises with to without the bending magnet operated corresponds to the neutralization efficiency. Figure 10 shows the neutralization efficiency measured using different three thermocouples as a function of the gas pressure in the beam transport region. The beam energy is 95 keV. A result of the theoretical calculation is also indicated by a dotted line in the figure. Although the measured neutralization efficiency is a little higher than the calculated one, relatively good agreement is found.

4. Discussion

The ratio of the acceleration current to the H^- ion current, I_{acc}/I_{H^-}, is required to be low, in order to reduce the thermal load of the grids and the beamline components and to raise the H^- acceleration efficiency of the acceleration power supplies. In this source this ratio is not less than at least 1.7 as shown in Figs. 2 and 3. The higher operational gas pressure causes the larger stripping loss of the accelerated H^- ions, that results in the higher ratio of the I_{acc}/I_{H^-}. As shown in Fig. 4, the calculated stripping loss is small during the beam acceleration. In the experiments, the ratio of the second to the first acceleration currents, I_{acc2}/I_{acc1}, is 0.95-1.0, that indicates that the stripping loss is small during the acceleration. The direct acceleration of the extracted electrons is small from the experimental results in the single-stage acceleration [6]. The secondary electrons produced by the incident H^- ions on the extraction grid and the electron suppression grid can be accelerated. The electron suppression grid is electrically connected to the extraction grid in the normal operation, and works to prevent the acceleration electric field from applying the extraction grid. As a result, the acceleration of secondary electrons produced on the extraction grid is expected to be suppressed to some extent. The secondary electrons produced on the electron suppression grid would be accelerated and contribute the large ratio of the I_{acc}/I_{H^-}. The aspect ratio of the extraction gap is so large and the extraction grid is so thick that the extracted H^- ion beam would diverge and a part of it would be incident on the extraction grid and the electron suppression grid. On the other hand, the beam spots corresponding to the grid apertures are observed on the back plate of the arc chamber. These seem to be marked by the back-streaming positive ions. The back-streaming positive ions would

also contribute the acceleration drain current. From the above discussion, the reduction of the incident H^- ions on the extraction grid and the electron suppression grid is important to reduce the I_{acc}/I_{H^-}. The larger end aperture on the downstream side of the extraction grid and the smaller aspect ratio of the extraction gap could be effective. The reduction of the back-streaming positive ions is also important. The positive ion suppression grid biased positively with respect to the grounded grid may be required on the upstream side of the grounded grid.

From Figs. 7-9, it is recognized that the optimum beam acceleration of H^- ions is achieved in the case of nearly the same electric fields in the first and the second acceleration gaps, on condition that the E_{acc1}/E_{ext} is adjusted for the aspect ratio of the extraction gap. Therefore, the single-gap high-energy acceleration is possible for an intense negative ion beam.

5. Concluding Remarks

High-energy acceleration of an intense negative ion beam has been performed with the two-stage acceleration using the 1/3-scaled external filter-type large negative ion source. The accelerated H^- ion current increases according to the 3/2 power of the total beam energy at the arc efficiency of 0.1 A/kW. As a result, a 13.6 A of the H^- ion current was accelerated to 125 keV. The stripping loss of the H^- ions during the acceleration is small, several %, due to the low gas pressure operation at less than 3.5 mTorr. The uniformity of the beam profile is not so good, and the beam divergent angle is estimated at 14-16 mrad from the profile fitting with multi-beamlets. The improvement of the beam

uniformity and the divergent angle is an important issue for the neutral beam application. The optimum beam acceleration conditions are found with regard to the electric field ratio of the first and the second acceleration. Nearly the same electric field in each acceleration stage realizes the optimum beam acceleration when the ratio of the first acceleration to the extraction electric fields is adjusted according to the aspect ratio of the extraction gap. The neutralization efficiency of the high-energy negative ions was measured and found to agree with the theoretical calculation.

It is concluded that these results presented here enable to design the actual LHD-NBI system with the negative ion beam.

Acknowledgements

The authors would like to greatly acknowledge Professor A. Iiyoshi, Director-General, for his continuous encouragement and support to the development of the ion source.

References

[1] T. Nagashima, R. S. Hemsworth, M. Makowski, D. Remsen, and the ITER Joint Central Team and Home Teams, *Proc. of the 15th Int. Conf. on Plasma Physics and Controlled Nuclear Fusion Research, Seville, Spain, 1994*, IAEA-CN-60/E-P-9.

[2] Y. Okumura, M. Hanada, T. Inoue, H. Kojima, Y. Matsuda, Y. Ohara, Y. Oohara, M. Seki, Y. Suzuki and K. Watanabe, *Proc. of the 16th Symp. on Fusion Technology, London, 1990*, p. 1026.

[3] Y. Okumura, M. Hanada, T. Inoue, H. Kojima, Y. Matsuda, Y. Ohara, M. Seki and K. Watanabe, *Proc. of the 5th Int. Symp. on the Production and Neutralization of Negative Ions and Beams, Upton, NY, 1990*, AIP Conf. Proc. No. 210, p. 169.

[4] A. Ando, Y. Takeiri, K. Tsumori, O. Kaneko, Y. Oka, R. Akiyama, T. Kawamoto, K. Mineo, T. Kurata and T. Kuroda, Rev. Sci. Instrum. **63**, 2683 (1992).

[5] A. Ando, K. Tsumori, Y. Oka, O. Kaneko, Y. Takeiri, E. Asano, T. Kawamoto, R. Akiyama and T. Kuroda, Phys. Plasmas **1**, 2813 (1994).

[6] Y. Takeiri, A. Ando, O. Kaneko, Y. Oka, K. Tsumori, R. Akiyama, E. Asano, T. Kawamoto, T. Kuroda, M. Tanaka and H. Kawakami, to be published in Rev. Sci. Instrum. **66**, No. 3 (1995).

[7] Y. Takeiri, A. Ando, O. Kaneko, Y. Oka, K. Tsumori, T. Takanashi, R. Akiyama, E. Asano, T. Kawamoto, M. Tanaka, H. Kawakami, T. Okuyama, Y. Suzuki and T. Kuroda, *Proc. of the 18th Symposium on Fusion Technology, Karlsruher, 1994*, to be published.

[8] K. Miyamoto, M. Hanada, T. Inoue, N. Miyamoto, A. Nagase, Y. Ohara, Y. Okumura and K. Watanabe, *Proc. of the 18th Symposium on Fusion Technology, Karlsruher, 1994*, to be published.

[9] J. Pamela, M. Fumelli, F. Jequier, A. Simonin, M. Hanada, Y. Okumura and K. Watanabe, *Proc. of the 6th Int. Symp. on Production and Neutralization of Negative Ions and Beams, Upton, NY, 1992*, AIP Conf. Proc. No. 287, p. 695.

[10] A. Iiyoshi, M. Fujiwara, O. Motojima, N. Ohyabu and K. Yamazaki, Fusion Technology **17**, 169 (1990).

[11] Y. Takeiri, O. Kaneko, F. Sano, A. Ando, Y. Oka, K. Hanatani, T. Obiki and T. Kuroda, *Proc. of the first Int. Toki Conf. on Plasma Physics and Controlled Nuclear Fusion, Toki, Japan, 1989*, p. 272.

[12] Y. Oka, A. Ando, O. Kaneko, Y. Takeiri, K. Tsumori, R. Akiyama, T. Kawamoto, K. Mineo, T. Kurata and T. Kuroda, *Proc. of the 14th Symp. on Fusion Engineering, San Diego, 1991*, p. 70.

[13] O. Kaneko, A. Ando, Y. Oka, Y. Takeiri, K. Tsumori, R. Akiyama, T. Kawamoto, T. Kurata, K. Mineo and T. Kuroda, *Proc. of the 17th Symp. on Fusion Technology, Rome, 1992*, p. 544.

[14] Y. Takeiri, A. Ando, O. Kaneko, Y. Oka, K. Tsumori, R. Akiyama, T. Kawamoto and T. Kuroda, *Proc. of the 6th Int. Symp. on Production and Neutralization of Negative Ions and Beams, Upton, NY, 1992*, AIP Conf. Proc. No. 287, p. 869.

[15] Y. Takeiri, Y. Oka, O. Kaneko, A. Ando, K. Tsumori, R. Akiyama, T. Kawamoto and T. Kuroda, Rev. Sci. Instrum. **65**, 1198 (1994).

[16] T. Inoue, M. Hanada, M. Mizuno, Y. Ohara, Y. Okumura, Y. Suzuki, M. Tanaka and K. Watanabe, *Proc. of the 6th Int. Symp. on Production and Neutralization of Negative Ions and Beams, Upton, NY, 1992*, AIP Conf. Proc. No. 287, p. 316.

Figure Captions

Fig. 1 (a) Schematic diagram of an external-filter type 1/3-scaled negative ion source, and (b) the grid arrangement along the beam axis and the electrical connections of the power supplies.

Fig. 2 (a) H^- ion current (open circles) and the second acceleration drain current (open triangles) as a function of the arc power, and (b) H^- ion current as a function of the total beam energy. A dashed line indicates the 3/2-power dependency on the beam energy. The gas pressure is 3.4 mTorr.

Fig. 3 (a) Arc efficiency of the H^- ions, and (b) the ratio of the extraction current to the H^- ion current, I_{ext}/I_{H^-}, (open circles) and the ratio of the second acceleration current to the H^- ion current, I_{acc2}/I_{H^-}, (open triangles) as a function of the gas pressure. The arc power is 90 to 100 kW and the H^- ion beam energy is 113 keV.

Fig. 4 Simulation results of the gas pressure distribution and the survival H^- ion ratio without the stripping loss in the accelerator using a Monte-Carlo gas flow calculation code.

Fig. 5 Contours of the H^- ion beam current density measured by scanning the calorimeter array. The arc power is 90 kW. The beam energy is 109 keV and the total H^- ion current is 9.6 A. The equi-current density lines are 0.93 mA/cm^2 units.

Fig. 6 Horizontal (X) profile of the H^- ion beam. The arc power is 88 kW. The beam energy is 110 keV and the total H^- ion current is 8.5 A. A calculated beam profile using the multi-gaussian beamlets with the divergent angle of 16 mrad is also shown by a dotted line.

Fig. 7 (a) FWHM of the horizontal profile, and (b) the H^- ion current (open circles) and the ratio of the second acceleration current to the H^- ion current, I_{acc2}/I_{H^-}, (open triangles) as a function of the ratio of the second to the first acceleration electric fields, E_{acc2}/E_{acc1}. The ratio of the first acceleration to the extraction electric fields, E_{acc1}/E_{ext}, is constant, 0.98. The extraction gap length is 3 mm. The arc power is 90 kW and the gas pressure is 3.4 mTorr.

Fig. 8 (a) FWHM of the horizontal profile, (b) the H^- ion current, and (c) the ratio of the second acceleration current to the H^- ion current, I_{acc2}/I_{H^-}, as a function of the ratio of the first acceleration to the extraction electric fields, E_{acc1}/E_{ext}. The parameter is the ratio of the second to the first acceleration electric fields, E_{acc2}/E_{acc1}, and the data are plotted for E_{acc2}/E_{acc1} = 0.9 (open squares), 1.05 (open circles) and 1.15 (open triangles). The extraction gap length is 3 mm. The arc power is 90 kW and the gas pressure is 3.4 mTorr.

Fig. 9 (a) FWHM of the horizontal profile, and (b) the arc efficiency (open circles) and the ratio of the second acceleration current to the H^- ion current, I_{acc2}/I_{H^-}, (open triangles) as a function of the ratio of the second to the first acceleration electric fields, E_{acc2}/E_{acc1}. The extraction gap length is 5 mm. The ratio of the first acceleration to the extraction electric fields, E_{acc1}/E_{ext}, is 1.18. The arc power is 90 kW and the gas pressure is 4 mTorr.

Fig.10 Neutralization efficiency measured as a function of the gas pressure in the beam transport region. A theoretical calculation result is indicated by a dotted line. The beam energy is 95 keV.

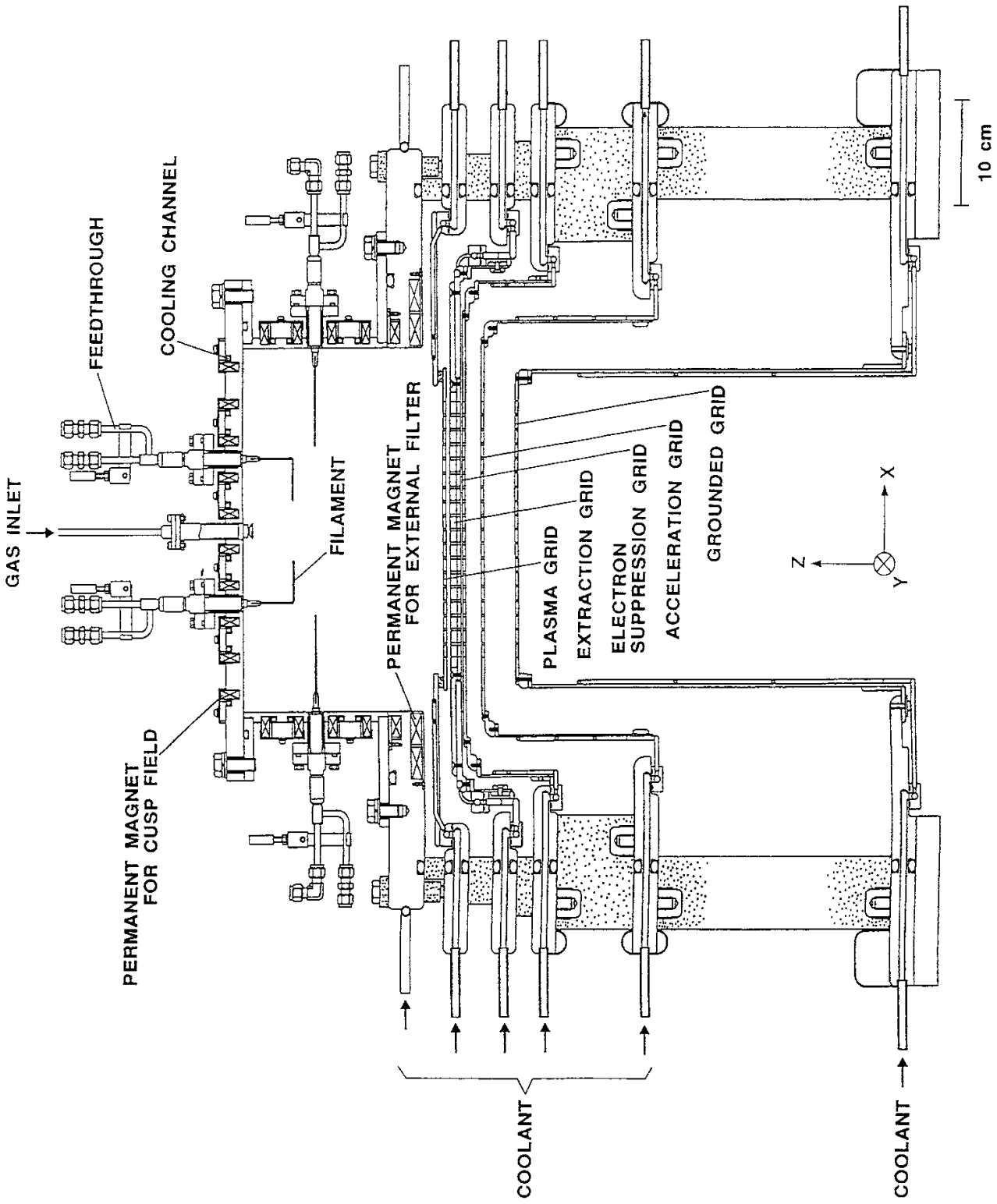

Figure 1 (a)
Y. Takeiri *et al.*

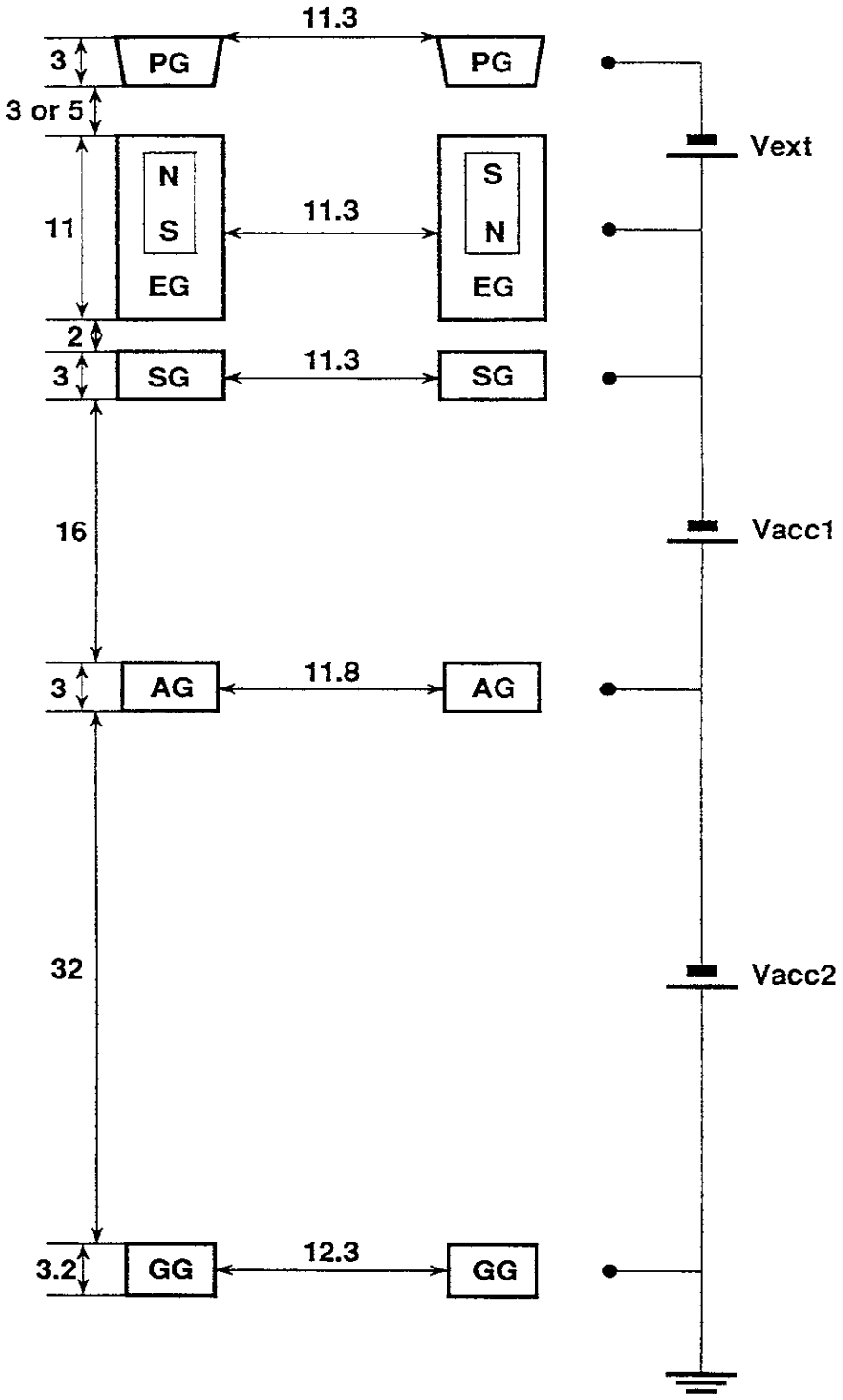

Figure 1 (b)
Y. Takeiri *et al.*

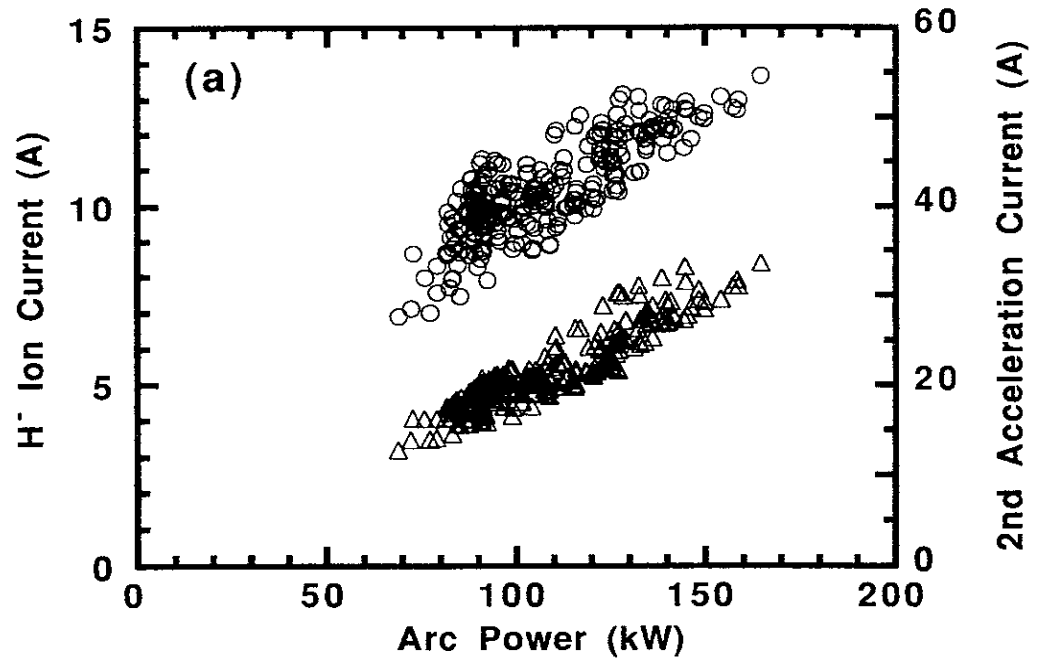

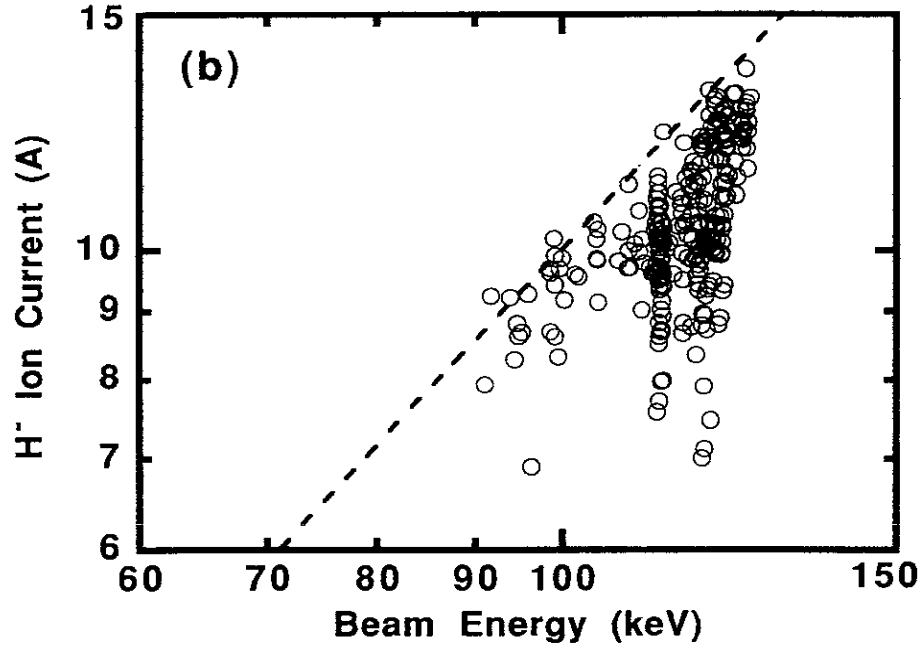

Figure 2
Y. Takeiri *et al.*

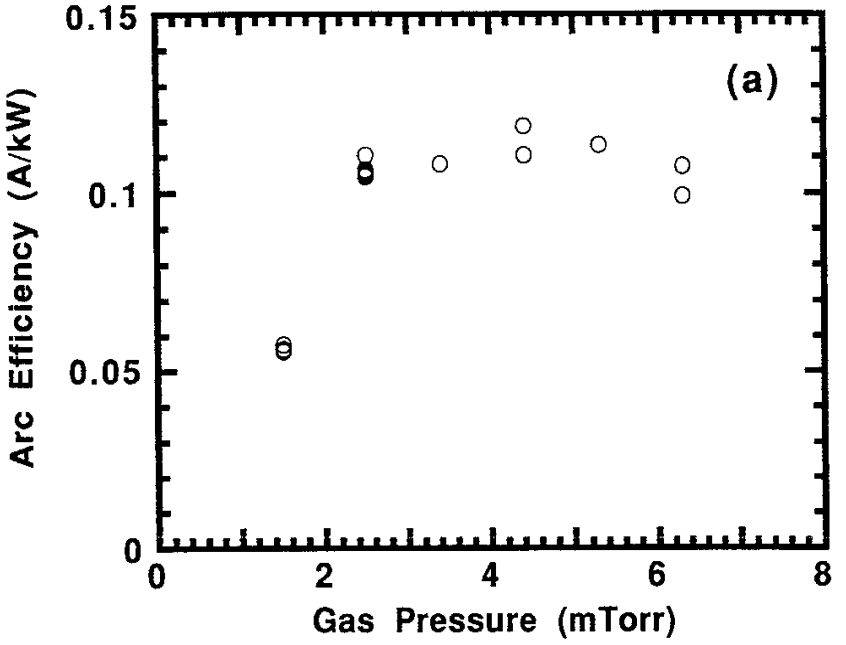

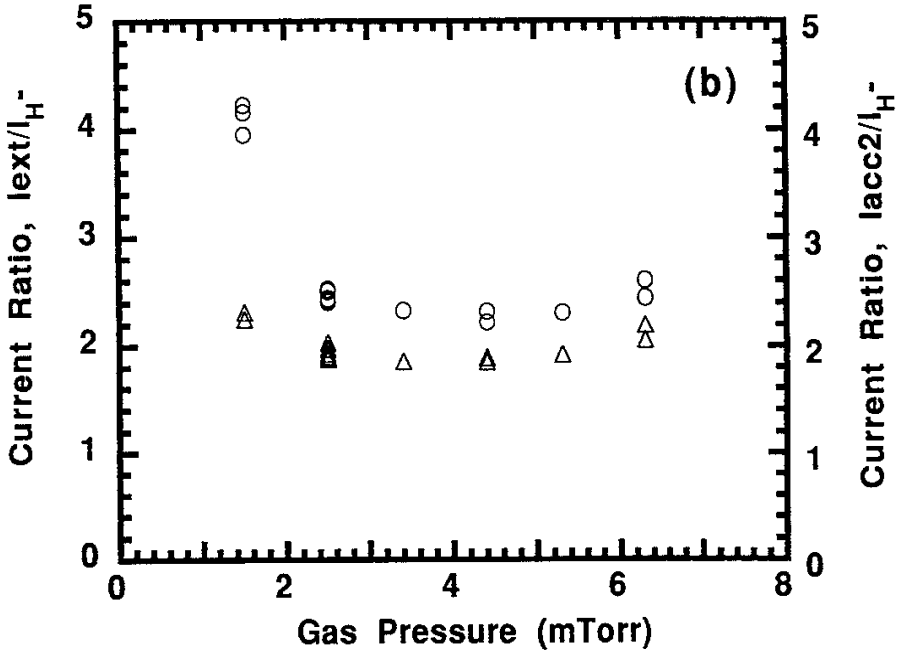

Figure 3
Y. Takeiri *et al.*

Figure 4
Y. Takeiri *et al.*

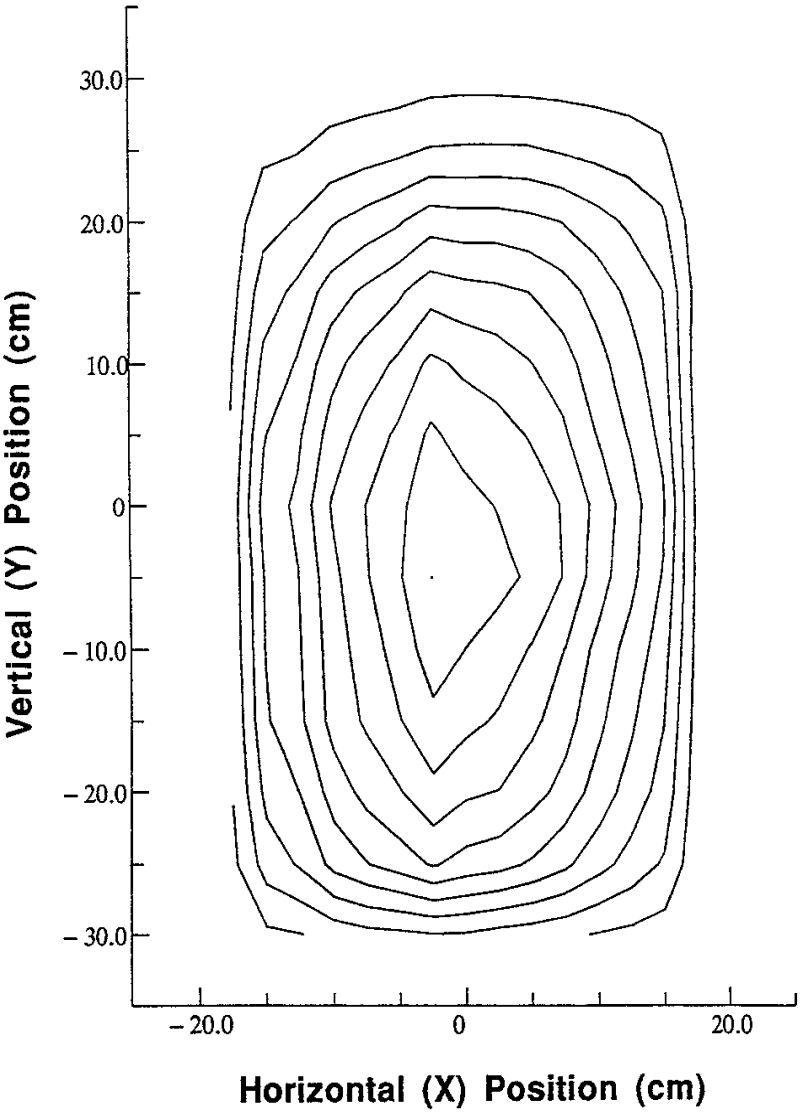

Figure 5
Y. Takeiri *et al.*

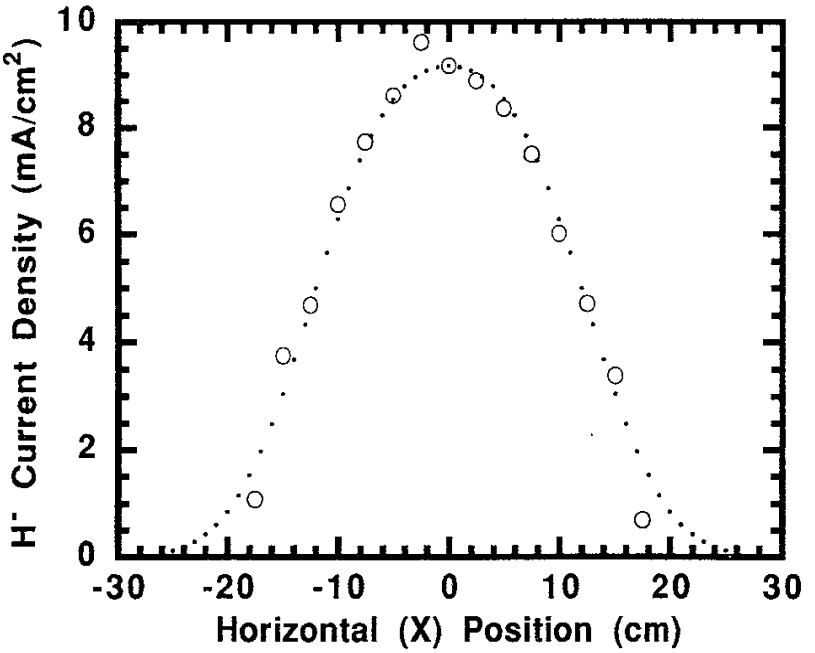

Figure 6
Y. Takeiri *et al.*

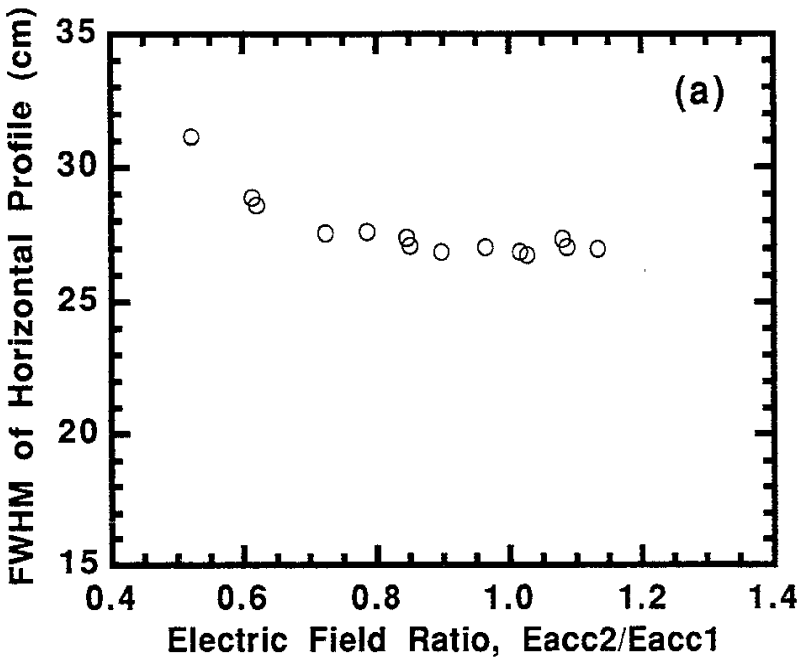

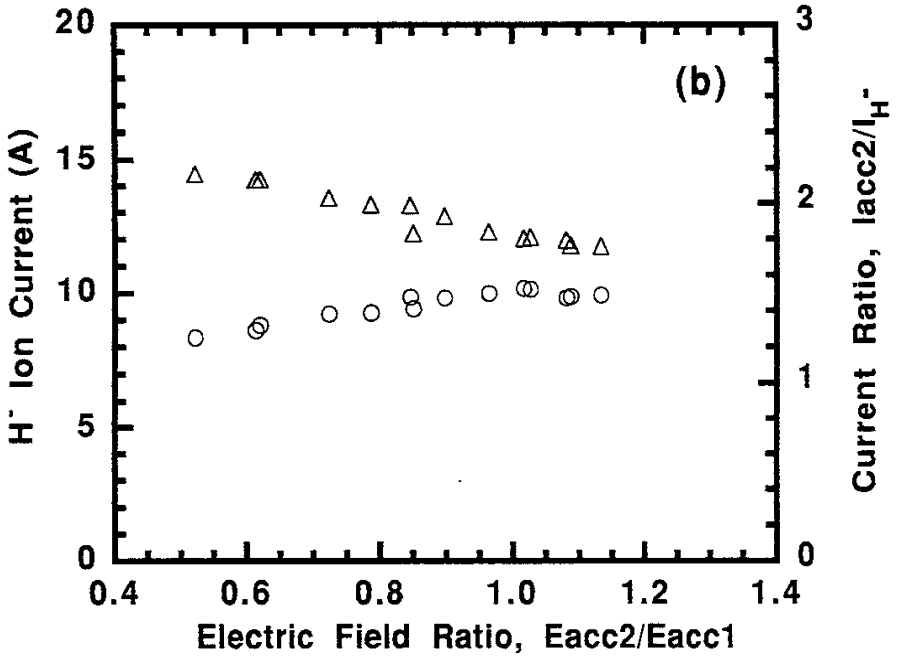

Figure 7
Y. Takeiri *et al.*

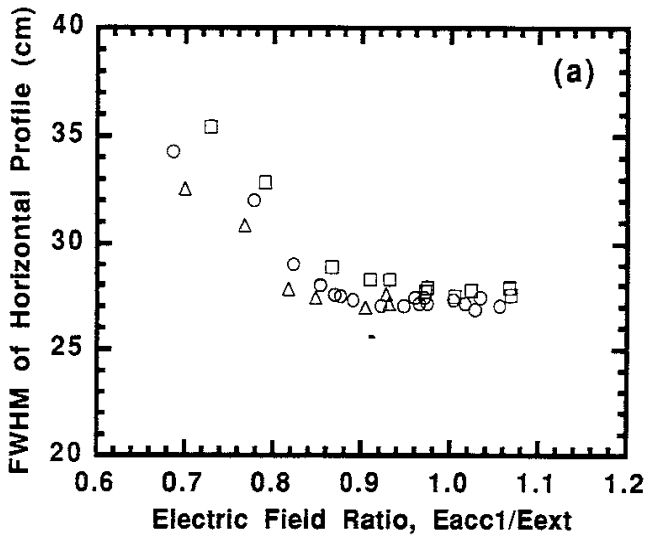

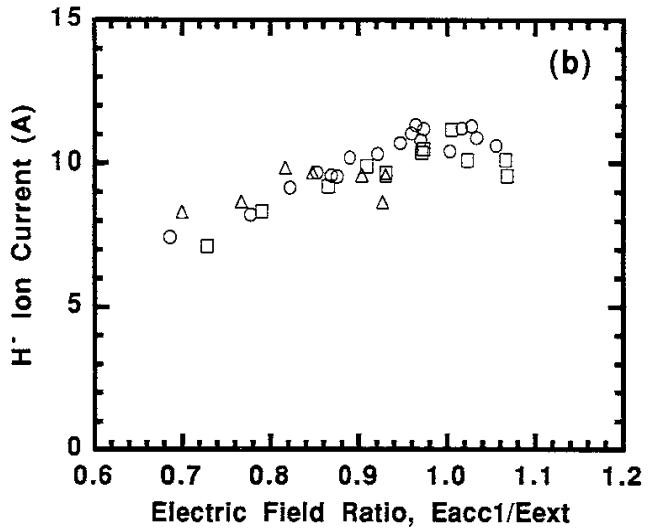

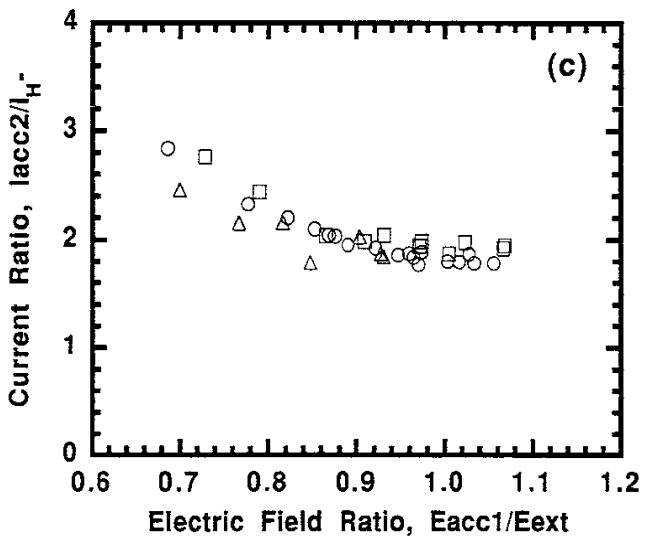

Figure 8
Y. Takeiri *et al.*

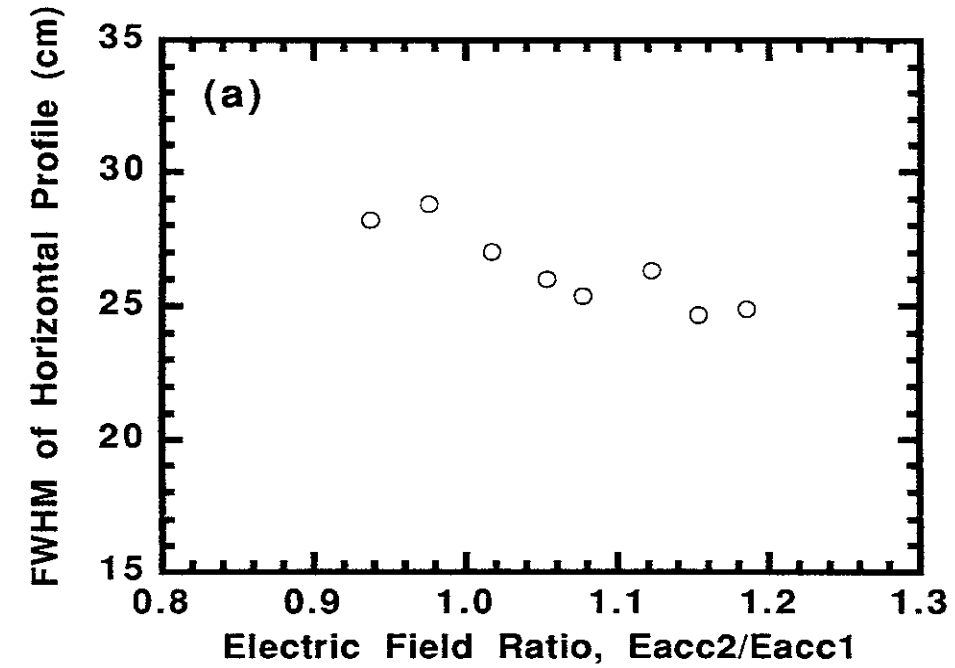

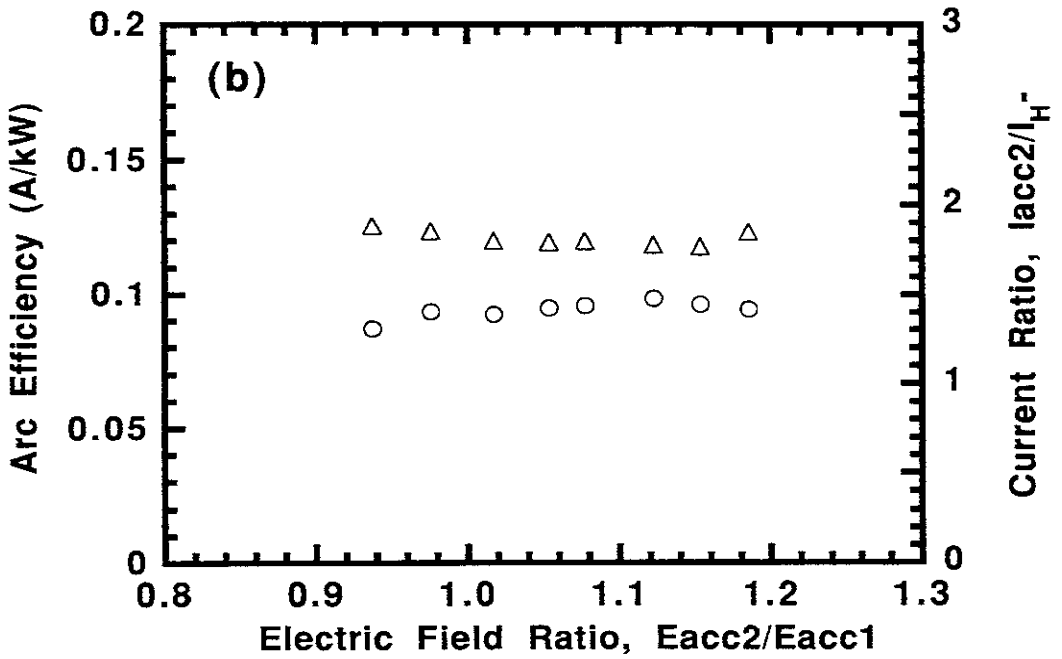

Figure 9
Y. Takeiri *et al.*

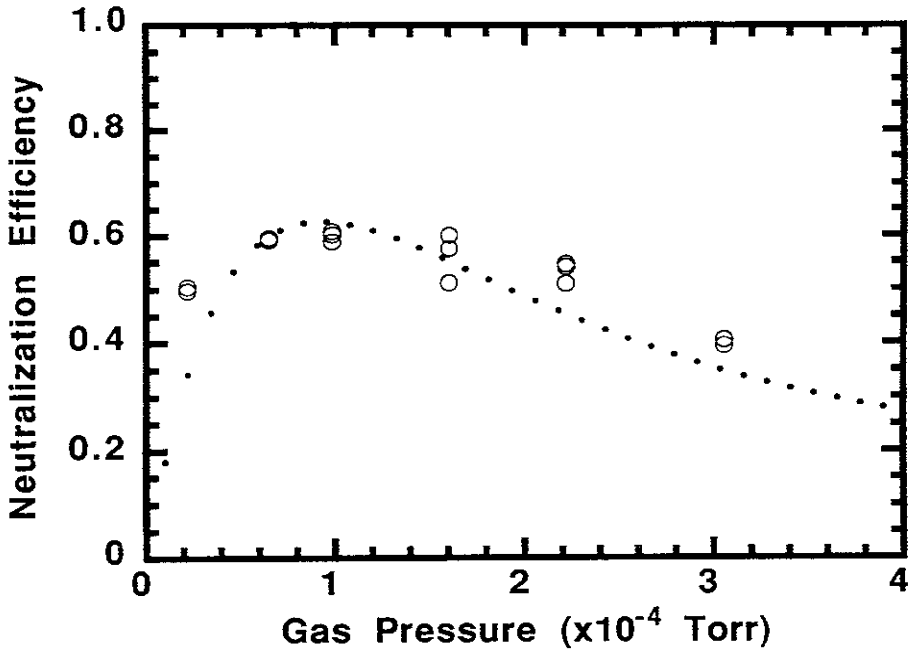

Figure 10
Y. Takeiri *et al.*

Recent Issues of NIFS Series

NIFS-296 K. Itoh, M. Yagi, S.-I. Itoh, A. Fukuyama, H. Sanuki, M. Azumi,
Anomalous Transport Theory for Toroidal Helical Plasmas,
Aug. 1994 (IAEA-CN-60/D-III-3)

NIFS-297 J. Yamamoto, O. Motojima, T. Mito, K. Takahata, N. Yanagi, S. Yamada,
H. Chikaraishi, S. Imagawa, A. Iwamoto, H. Kaneko, A. Nishimura, S. Satoh,
T. Satow, H. Tamura, S. Yamaguchi, K. Yamazaki, M. Fujiwara, A. Iiyoshi
and LHD group,
New Evaluation Method of Superconductor Characteristics for Realizing the Large Helical Device; Aug. 1994 (IAEA-CN-60/F-P-3)

NIFS-298 A. Komori, N. Ohyabu, T. Watanabe, H. Suzuki, A. Sagara, N. Noda,
K. Akaishi, N. Inoue, Y. Kubota, O Motojima, M. Fujiwara and A. Iiyoshi,
Local Island Divertor Concept for LHD; Aug. 1994 (IAEA-CN-60/F-P-4)

NIFS-299 K. Toi, T. Morisaki, S. Sakakibara, A. Ejiri, H. Yamada, S. Morita,
K. Tanaka, N. Nakajima, S. Okamura, H. Iguchi, K. Ida, K. Tsumori,
S. Ohdachi, K. Nishimura, K. Matsuoka, J. Xu, I. Yamada, T. Minami,
K. Narihara, R. Akiyama, A. Ando, H. Arimoto, A. Fujisawa, M. Fujiwara,
H. Idei, O. Kaneko, K. Kawahata, A. Komori, S. Kubo, R. Kumazawa,
T. Ozaki, A. Sagara, C. Takahashi, Y. Takita and T. Watari,
Impact of Rotational-Transform Profile Control on Plasma Confinement and Stability in CHS; Aug. 1994 (IAEA-CN-60/A6/C-P-3)

NIFS-300 H. Sugama and W. Horton,
Dynamical Model of Pressure-Gradient-Driven Turbulence and Shear Flow Generation in L-H Transition; Aug. 1994 (IAEA/CN-60/D-P-I-11)

NIFS-301 Y. Hamada, A. Nishizawa, Y. Kawasumi, K.N. Sato, H. Sakakita, R. Liang,
K. Kawahata, A. Ejiri, K. Narihara, K. Sato, T. Seki, K. Toi, K. Itoh,
H. Iguchi, A. Fujisawa, K. Adachi, S. Hidekuma, S. Hirokura, K. Ida,
M. Kojima, J. Koog, R. Kumazawa, H. Kuramoto, T. Minami, I. Negi,
S. Ohdachi, M. Sasao, T. Tsuzuki, J. Xu, I. Yamada, T. Watari,
Study of Turbulence and Plasma Potential in JIPP T-IIU Tokamak;
Aug. 1994 (IAEA/CN-60/A-2-III-5)

NIFS-302 K. Nishimura, R. Kumazawa, T. Mutoh, T. Watari, T. Seki, A. Ando,
S. Masuda, F. Shinpo, S. Murakami, S. Okamura, H. Yamada, K. Matsuoka,
S. Morita, T. Ozaki, K. Ida, H. Iguchi, I. Yamada, A. Ejiri, H. Idei, S. Muto,
K. Tanaka, J. Xu, R. Akiyama, H. Arimoto, M. Isobe, M. Iwase, O. Kaneko,
S. Kubo, T. Kawamoto, A. Lazaros, T. Morisaki, S. Sakakibara, Y. Takita,
C. Takahashi and K. Tsumori,
ICRF Heating in CHS; Sep. 1994 (IAEA-CN-60/A-6-I-4)

NIFS-303 S. Okamura, K. Matsuoka, K. Nishimura, K. Tsumori, R. Akiyama,
S. Sakakibara, H. Yamada, S. Morita, T. Morisaki, N. Nakajima, K. Tanaka,

J. Xu, K. Ida, H. Iguchi, A. Lazaros, T. Ozaki, H. Arimoto, A. Ejiri, M. Fujiwara, H. Idei, A. Iiyoshi, O, Kaneko, K. Kawahata, T. Kawamoto, S. Kubo, T. Kuroda, O. Motojima, V.D. Pustovitov, A. Sagara, C. Takahashi, K. Toi and I. Yamada,
High Beta Experiments in CHS; Sep. 1994 (IAEA-CN-60/A-2-IV-3)

NIFS-304 K. Ida, H. Idei, H. Sanuki, K. Itoh, J. Xu, S. Hidekuma, K. Kondo, A. Sahara, H. Zushi, S.-I. Itoh, A. Fukuyama, K. Adati, R. Akiyama, S. Bessho, A. Ejiri, A. Fujisawa, M. Fujiwara, Y. Hamada, S. Hirokura, H. Iguchi, O. Kaneko, K. Kawahata, Y. Kawasumi, M. Kojima, S. Kubo, H. Kuramoto, A. Lazaros, R. Liang, K. Matsuoka, T. Minami, T. Mizuuchi, T. Morisaki, S. Morita, K. Nagasaki, K. Narihara, K. Nishimura, A. Nishizawa, T. Obiki, H. Okada, S. Okamura, T. Ozaki, S. Sakakibara, H. Sakakita, A. Sagara, F. Sano, M. Sasao, K. Sato, K.N. Sato, T. Saeki, S. Sudo, C. Takahashi, K. Tanaka, K. Tsumori, H.Yamada, I. Yamada, Y. Takita, T. Tuzuki, K. Toi and T. Watari,
Control of Radial Electric Field in Torus Plasma; Sep. 1994
(IAEA-CN-60/A-2-IV-2)

NIFS-305 T. Hayashi, T. Sato, N. Nakajima, K. Ichiguchi, P. Merkel, J. Nührenberg, U. Schwenn, H. Gardner, A. Bhattacharjee and C.C.Hegna,
Behavior of Magnetic Islands in 3D MHD Equilibria of Helical Devices;
Sep. 1994 (IAEA-CN-60/D-2-II-4)

NIFS-306 S. Murakami, M. Okamoto, N. Nakajima, K.Y. Watanabe, T. Watari, T. Mutoh, R. Kumazawa and T. Seki,
Monte Carlo Simulation for ICRF Heating in Heliotron/Torsatrons;
Sep. 1994 (IAEA-CN-60/D-P-I-14)

NIFS-307 Y. Takeiri, A. Ando, O. Kaneko, Y. Oka, K. Tsumori, R. Akiyama, E. Asano, T. Kawamoto, T. Kuroda, M. Tanaka and H. Kawakami,
Development of an Intense Negative Hydrogen Ion Source with a Wide-Range of External Magnetic Filter Field; Sep. 1994

NIFS-308 T. Hayashi, T. Sato, H.J. Gardner and J.D. Meiss,
Evolution of Magnetic Islands in a Heliac; Sep. 1994

NIFS-309 H. Amo, T. Sato and A. Kageyama,
Intermittent Energy Bursts and Recurrent Topological Change of a Twisting Magnetic Flux Tube; Sep.1994

NIFS-310 T. Yamagishi and H. Sanuki,
Effect of Anomalous Plasma Transport on Radial Electric Field in Torsatron/Heliotron; Sep. 1994

NIFS-311 K. Watanabe, T. Sato and Y. Nakayama,
Current-profile Flattening and Hot Core Shift due to the Nonlinear Development of Resistive Kink Mode; Oct. 1994

NIFS-312 M. Salimullah, B. Dasgupta, K. Watanabe and T. Sato,
Modification and Damping of Alfvén Waves in a Magnetized Dusty Plasma; Oct. 1994

NIFS-313 K. Ida, Y. Miura, S -I. Itoh, J.V. Hofmann, A. Fukuyama, S. Hidekuma, H. Sanuki, H. Idei, H. Yamada, H. Iguchi, K. Itoh,
Physical Mechanism Determining the Radial Electric Field and its Radial Structure in a Toroidal Plasma; Oct. 1994

NIFS-314 Shao-ping Zhu, R. Horiuchi, T. Sato and The Complexity Simulation Group,
Non-Taylor Magnetohydrodynamic Self-Organization; Oct. 1994

NIFS-315 M. Tanaka,
Collisionless Magnetic Reconnection Associated with Coalescence of Flux Bundles; Nov. 1994

NIFS-316 M. Tanaka,
Macro-EM Particle Simulation Method and A Study of Collisionless Magnetic Reconnection; Nov. 1994

NIFS-317 A. Fujisawa, H. Iguchi, M. Sasao and Y. Hamada,
Second Order Focusing Property of 210° Cylindrical Energy Analyzer; Nov. 1994

NIFS-318 T. Sato and Complexity Simulation Group,
Complexity in Plasma - A Grand View of Self- Organization; Nov. 1994

NIFS-319 Y. Todo, T. Sato, K. Watanabe, T.H. Watanabe and R. Horiuchi,
MHD-Vlasov Simulation of the Toroidal Alfvén Eigenmode; Nov. 1994

NIFS-320 A. Kageyama, T. Sato and The Complexity Simulation Group,
Computer Simulation of a Magnetohydrodynamic Dynamo II: Nov. 1994

NIFS-321 A. Bhattacharjee, T. Hayashi, C.C.Hegna, N. Nakajima and T. Sato,
Theory of Pressure-induced Islands and Self-healing in Three-dimensional Toroidal Magnetohydrodynamic Equilibria; Nov. 1994

NIFS-322 A. Iiyoshi, K. Yamazaki and the LHD Group,
Recent Studies of the Large Helical Device; Nov. 1994

NIFS-323 A. Iiyoshi and K. Yamazaki,
The Next Large Helical Devices; Nov. 1994

NIFS-324 V.D. Pustovitov
Quasisymmetry Equations for Conventional Stellarators; Nov. 1994

NIFS-325 A. Taniike, M. Sasao, Y. Hamada, J. Fujita, M. Wada,
The Energy Broadening Resulting from Electron Stripping Process of a Low Energy Au^- Beam; Dec. 1994

NIFS-326 I. Viniar and S. Sudo,
New Pellet Production and Acceleration Technologies for High Speed Pellet Injection System "HIPEL" in Large Helical Device; Dec. 1994

NIFS-327 Y. Hamada, A. Nishizawa, Y. Kawasumi, K. Kawahata, K. Itoh, A. Ejiri, K. Toi, K. Narihara, K. Sato, T. Seki, H. Iguchi, A. Fujisawa, K. Adachi, S. Hidekuma, S. Hirokura, K. Ida, M. Kojima, J. Koong, R. Kumazawa, H. Kuramoto, R. Liang, T. Minami, H. Sakakita, M. Sasao, K.N. Sato, T. Tsuzuki, J. Xu, I. Yamada, T. Watari,
Fast Potential Change in Sawteeth in JIPP T-IIU Tokamak Plasmas; Dec. 1994

NIFS-328 V.D. Pustovitov,
Effect of Satellite Helical Harmonics on the Stellarator Configuration; Dec. 1994

NIFS-329 K. Itoh, S-I. Itoh and A. Fukuyama,
A Model of Sawtooth Based on the Transport Catastrophe; Dec. 1994

NIFS-330 K. Nagasaki, A. Ejiri,
Launching Conditions for Electron Cyclotron Heating in a Sheared Magnetic Field; Jan. 1995

NIFS-331 T.H. Watanabe, Y. Todo, R. Horiuchi, K. Watanabe, T. Sato,
An Advanced Electrostatic Particle Simulation Algorithm for Implicit Time Integration; Jan. 1995

NIFS-332 N. Bekki and T. Karakisawa,
Bifurcations from Periodic Solution in a Simplified Model of Two-dimensional Magnetoconvection; Jan. 1995

NIFS-333 K. Itoh, S.-I. Itoh, M. Yagi, A. Fukuyama,
Theory of Anomalous Transport in Reverse Field Pinch; Jan. 1995

NIFS-334 K. Nagasaki, A. Isayama and A. Ejiri
Application of Grating Polarizer to 106.4GHz ECH System on Heliotron-E; Jan. 1995

NIFS-335 H. Takamaru, T. Sato, R. Horiuchi, K. Watanabe and Complexity Simulation Group,
A Self-Consistent Open Boundary Model for Particle Simulation in Plasmas; Feb. 1995

NIFS-336 B.B. Kadomtsev,
Quantum Telegragh : is it possible?; Feb. 1995

NIFS-337 B.B.Kadomtsev,
Ball Lightning as Self-Organization Phenomenon; Feb. 1995